Realization of Nonlinear Real-Time Optimization Based Controllers on Self-Contained Transfemoral Prosthesis

Huihua Zhao
Mechanical Engineering
Texas A&M University
College Station, USA
huihuazhao@tamu.edu

Jake Reher
Mechanical Engineering
Texas A&M University
College Station, USA
jreher@tamu.edu

Jonathan Horn
Mechanical Engineering
Texas A&M University
College Station, USA
j.horn@tamu.edu

Victor Paredes
Mechanical Engineering
Texas A&M University
College Station, USA
vcparedesc@tamu.edu

Aaron D. Ames
Mechanical Engineering
Texas A&M University
College Station, USA
aames@tamu.edu

ABSTRACT

Lower-limb prosthesis provide a prime example of cyber-physical systems (CPSs) that interact with humans in a safety critical fashion, and therefore require the synergistic development of sensing, algorithms and controllers. With a view towards better understanding CPSs of this form, this paper presents a methodology for successfully translating nonlinear real-time optimization based controllers from bipedal robots to a novel custom built self-contained powered transfemoral prosthesis: AMPRO. To achieve this goal, we begin by collecting reference human locomotion data via Inertial measurement Units (IMUs). This data forms the basis for an optimization problem that generates virtual constraints, i.e., parametrized trajectories, for the prosthesis that provably yields walking in simulation. Utilizing methods that have proven successful in generating stable robotic locomotion, control Lyapunov function (CLF) based Quadratic Programs (QPs) are utilized to optimally track the resulting desired trajectories. The parameterization of the trajectories is determined through a combination of on-board sensing on the prosthesis together with IMU data, thereby coupling the actions of the user with the controller. Finally, impedance control is integrated into the QP yielding an optimization based control law that displays remarkable tracking and robustness, outperforming traditional PD and impedance control strategies. This is demonstrated experimentally on AMPRO through the implementation of the holistic sensing, algorithm and control framework, with the end result being stable and human-like walking.

Figure 1: The novel Prosthesis AMPRO that is capable of running nonlinear optimization based controllers in real-time.

1. INTRODUCTION

As one of the most important applications of bipedal robotic research, powered lower-limb prosthesis is a prime example of cyber-physical systems (CPSs) that requires tight interaction between the able-body of the human and the prosthetic device in a safety critical fashion. During the course of a step, the human leg and the prosthetic device interchange roles between weight bearing (stance phase) and swing forward (swing phase) phases; therefore, a synergistic development of sensing, algorithms and controllers for the correct and safe collaboration between the human and the device are required. In particular, the prosthetic device must be able to bear human weight during stance phase and sense the human intention (to move accordingly) during swing phase. More importantly, the prosthesis must operate with an almost identical appearance when compared to a healthy human walking gait. The goal of this paper is to present a methodology for achieving these performance specifications via a nonlinear on-line optimization based controller. Additionally, it will be shown that the performance of the proposed controller outperforms traditional controllers such as proportional-derivative (PD) or variable impedance control.

The knee and ankle joints of healthy humans generate significant net power during daily locomotion [2, 31]. However, the current market for transfemoral prosthesis is dominated by passive pros-

thetic devices, limiting the day-to-day life of amputees (increased metabolic cost and constrained locomotion capabilities [30]). Motivated by this situation, the development of a powered prosthesis capable of providing net power in conjunction with various prosthesis controllers have been developed. Most notably, [14, 15] developed a hydraulically actuated knee prosthesis with the "echo control" method to mirror the modified trajectory of a healthy leg to the opposing side. Control based on gait-pattern generators has been realized in [16, 24]. Motion intent recognition with position control was successfully implemented in an ankle-foot prosthesis device in [11]. Under the assumption that the human gait is cyclic, variable impedance control is also one of the most common approaches for controlling prosthesis [10, 12, 13, 18, 28].

Impedance control assumes that the torque at each joint during a single step cycle can be represented by a series of passive impedance functions [17], [28]. By reproducing this torque at the prosthetic device joint, one can obtain prosthetic walking with similar gaits found in normal humans. However, due to hand tuning and the lack of feedback [9, 23], impedance control lacks both optimality and robustness. Motivated by these issues, an innovate controller that combines the rapidly exponentially stabilizing control Lyapunov functions (RES-CLFs) [6] with impedance control is proposed with the goal of achieving better tracking and improved robustness on prosthesis. This controller was first verified in simulation for flat-ground and up-slope walking in [32] and then tested on a bipedal robot which achieved stable "prosthetic" walking in [33], yet it has never been realized on an actual prosthesis.

In this work, we will present the complete methodology by which the proposed novel controller was explicitly implemented on a custom built self-contained transfemoral prosthesis to achieve stable prosthetic walking with a healthy human subject. We begin with the introduction of a motion capture system using Inertial Measurement Units (IMUs) to collect human locomotion trajectories. With the collected data, the human-inspired optimization problem [4] is then leveraged to obtain a stable and robust gait for a specific test subject. IMUs are then used to estimate human intention during walking thus providing human sensory feedback. With this systematic development (including sensing, algorithm and controllers) the end result is stable robust human-like prosthetic walking in both the laboratory and outside in real-world environments. Other different controllers (such as PD) are also tested on the prosthesis in order to compare the performance with the proposed controller. In addition to demonstrating the ability of the proposed controller, it is compared against existing control stratifies—the online optimization based controller is able to achieve better tracking with reduced torque and power consumption.

The structure of this paper is as follows: In Sec. 2, human locomotion data collection with IMUs is introduced. Based on the collected data, human-inspired optimization is utilized to obtain the optimized trajectories for the prosthesis. Utilizing RES-CLFs and impedance control, in Sec. 3 the novel *model independent quadratic program* (MIQP) based controller is introduced specifically with a view toward practical application. Finally, the experimental realization of the nonlinear on-line optimization based controller on a real prosthesis device is illustrated explicitly in Sec. 4. Conclusions and future work are presented at the end.

2. PROSTHETIC GAIT GENERATION

In an effort to achieve human-like robotic walking with a transfemoral robotic leg, an inertial motion capture system with IMUs is developed and interfaced with the human-inspired control approach [22]. In particular, this system is first used to capture the walking trajectories of the user. Utilizing the collected human locomotion data as the reference, a human-inspired optimization problem [22] is employed to design a stable and optimal gait which suits the specific test subject. The IMU system is then embedded on the user to interface with the controller in real-time to achieve prosthetic walking.

2.1 Motion Capture with IMU

In an effort to achieve human-like robotic walking, a motion capture system is developed with the purpose of collecting user locomotion trajectories. In particular, a model based Extended Kalman Filter (EKF) is introduced to obtain accurate joint angle information about the human subject.

Kinematics-Based Extended Kalman Filter. The algorithm implemented for motion capture is a modification of the model-based EKF first presented by [27]. In particular, the algorithm used in this work is different in two aspects: the kinematic model of the human legs is assumed to be two dimensional in the saggital plane and the kinematic chain is built from the hip. Before the filter can be implemented, sensor readings for each segment must be corrected. Attaching IMUs to the user is not ideal since the sensor frame of reference will not align with that of the kinematic link. A two step calibration procedure is performed to rotate sensor readings into the appropriate frame. Once the sensor frame has been corrected through calibration, the asssumption is made that the user will walk soley in the saggital plane and all three-dimensional sensor readings resulting in movement from this plane are negated.

To construct a model of the human leg, a kinematic chain must be built from a location which has either negligible acceleration, or from a location in which the acceleration is known. In the human-inspired control approach [4], the forward position of the hip is assumed to be linear in nature and is used as a phasing variable for gait progression. Due to the linear nature of the hip position in this approach, it is assumed in this model that the linear acceleration of the hip is approximately zero. This assumption allows each leg to be built from the hip rather than stance foot.

A two-link kinematic chain (one thigh, one shank) is built from the hip for each leg. The EKF is updated for each link in the model, providing an estimate of the angular velocity, angular acceleration, quaternion orientation, and the time derivative of the quaternion at each time step in the earth frame. The link state estimation is updated from the measurements performed on each link, including angular velocity, angular acceleration and linear acceleration. Each segment EKF then provides its individual earth frame orientation. As such, the quaternion product between any two connected links,

$$q_j = q_i^* \otimes q_{i+1}, \tag{1}$$

results in the joint rotation between any two links, where q^* denotes the quaternion conjugate, i is the link index from the hip, and j is the joint index. More details can be found in [19].

Human Trajectory Collection. During data collection, inertial sensing is performed by seven Invensense MPU-9150 devices consisting of a tri-axial gyroscope (range $\pm 500^0/s$) and a tri-axial accelerometer (range $\pm 4g$). Each IMU transfers angular velocity and acceleration readings to a microcontroller at a rate of 200 Hz for processing. The detailed setup of the IMUs is presented in [19]. During the experiment, the subject was asked to walk along a straight line in a flat-footed gait for several steps. The joint states are estimated and collected with the EKF algorithm, and then several steps are averaged to yield their unique trajectories for optimization. Note that the EKF algorithm is also used with the purpose of interaction between the human and prosthesis device and provides the feedback of human intention during walking. Detailed illustration of this usage will be discussed later in Sec. 4.

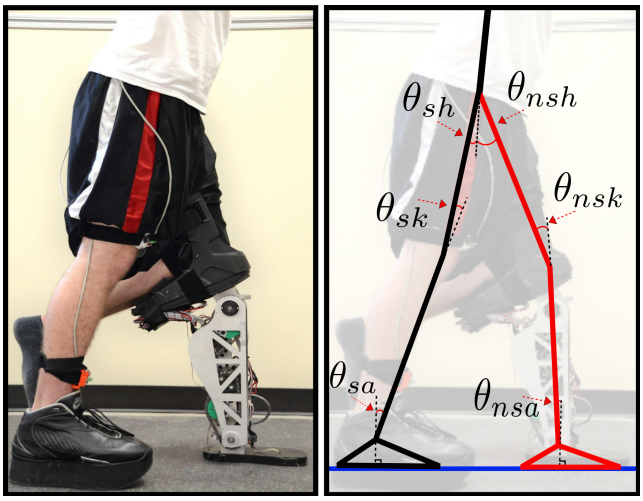

Figure 2: Robot Model including joint angles.

2.2 Gait Generation For Prosthetics

A methodology for designing a prosthetic gait that is specific to each individual user is now presented. In particular, a planar bipedal robot with anthropomorphic parameters is considered as the "human" model for the purpose of gait design in this work. Based on this model and the human locomotion data obtained with the IMUs, the human-inspired optimization [4] is implemented to generate a human-like gait that is both stable and optimal for the prosthetic device.

Robot Model. A seven-link planar bipedal robot (one torso, two thighs, two calves and two feet) with anthropomorphic parameters corresponding to the test subject, is considered as the "human" model in this work. Due to the existence of discrete behavior (when foot impacts the ground) present in walking, we represent the bipedal robot as a hybrid system with the configuration space Q_R defined as: $\theta = (\theta_{sa}, \theta_{sk}, \theta_{sh}, \theta_{nsh}, \theta_{nsk}, \theta_{nsa})^T$ as shown in Fig. 2. The equations of motion of the continuous dynamics are found using the Euler-Lagrange formula:

$$D(\theta)\ddot{\theta} + H(\theta, \dot{\theta}) = Bu, \tag{2}$$

where $D(\theta) \in \mathbb{R}^{6\times 6}$ is the inertial matrix and $H(\theta, \dot{\theta}) \in \mathbb{R}^{6\times 1}$ contains the terms resulting from the Coriolis effect $C(\theta, \dot{\theta})\dot{\theta}$ and the gravity vector $G(\theta)$. The torque map $B = I_6$ (under the assumption that the robot is fully-actuated) and the control input, u, is the vector of torque inputs. With the notation $x = (\theta; \dot{\theta})$, the affine control system $\dot{x} = f(x) + g(x)u$ can be obtained by reformulating (2) [26]. The discrete behavior of impact is modeled with the perfectly plastic impact assumption; more details can be found in [4], [20].

Human-Inspired Outputs. With the goal of achieving human-like bipedal robotic walking, we take the perspective of viewing the "complex" human locomotion system as a "black box." Therefore, the goal becomes to drive the actual robot outputs $y_a(\theta)$ to the desired human outputs $y_d(t, \alpha)$ that are represented by the *canonical walking function* (CWF) which is characterized with a parameter set α [4]. In particular, for the pinned-to-ground 7-link bipedal robot considered in this paper, a total of 6 outputs are of interest; for details, refer to [22]. Therefore, we introduce human-inspired outputs:

$$y(\theta, \dot{\theta}) = \begin{bmatrix} y_1(\theta, \dot{\theta}) \\ y_2(\theta) \end{bmatrix} = \begin{bmatrix} y_1^a(\theta, \dot{\theta}) - v_{hip} \\ y_2^a(\theta) - y_2^d(\rho(\theta), \alpha) \end{bmatrix}, \tag{3}$$

where $y_1(\theta, \dot{\theta})$ is the relative degree one output, which is the difference between the actual hip velocity $y_1^a(\theta, \dot{\theta})$ and the desired hip velocity v_{hip}. The vector $y_2(\theta)$ contains the relative degree two human-inspired outputs which are the differences between the actual outputs $y_2^a(\theta)$ and desired outputs $y_2^d(\rho(\theta), \alpha)$.

Upon observation of human locomotion data, the linearized forward hip position, $\delta p_{hip}(\theta)$, was discovered to increase linearly as a function of time; this motives the following phase variable:

$$\rho(\theta) = (\delta p_{hip}(\theta) - \delta p_{hip}^+)/v_{hip} \tag{4}$$

that will be used to parameterize a given walking gait. More importantly, this phase variable also serves as the key factor for interaction between the human and the device, the details of which will be discussed later. Note that, $\delta p_{hip}^+(\theta)$ is the initial linearized forward hip position at the beginning of a step, which will be decided through an *a priori* optimization problem.

Utilizing these outputs, the human-inspired controller [4] can be utilized to drive both $y_1 \to 0$ and $y_2 \to 0$ (corresponding to the *full zero dynamics surface* $\mathbf{FZ}_\alpha$ as defined in [4]) in a provably exponentially stable fashion. However, while the human-inspired controller renders exponential convergence for the continuous dynamics, the robot will be "thrown-off" the designed trajectory when impacts occur. This motivates the introduction of the *partial hybrid zero dynamics* (PHZD) constraints aiming to yield a parameter set α that ensures the tracking of relative degree two outputs will remain invariant even through impacts. In particular, with the *partial zero dynamics* (PZD) surface defined as:

$$\mathbf{PZ}_\alpha = \{(\theta, \dot{\theta}) \in TQ_R : y_2(\theta, \alpha) = \mathbf{0}, L_f y_2(\theta, \alpha) = \mathbf{0}\}, \tag{5}$$

the PHZD constraint can be explicitly stated as:

$$\Delta_R(S_R \cap \mathbf{FZ}_\alpha) = \mathbf{PZ}_\alpha, \tag{PHZD}$$

where Δ_R and S_R are the reset map and switching surface of the robot model, respectively. The detailed explanation of these constraints can be found in [4], [22].

Human-Inspired Optimization. By enforcing the PHZD constraint discussed above, the human-inspired optimization can be utilized to generate robot trajectories that are both provably stable and human-like [4], [34]. However, for the cyber-physical system of a lower-limb prosthesis interacting with humans in a safety critical fashion, more attention must be placed on physical constraints that relate to safety and energy conservation. One particular goal, for example, is to optimize the torque profile such that the motors are able to bear the human weight during the stance phase. More importantly, walking gaits that require smaller torques also decrease the energy consumption and, as a result, will prolong battery life. These specifications yield the optimization problem subject to PHZD and physical constraints::

$$\begin{aligned} \alpha^* = \underset{\alpha \in \mathbb{R}^{26}}{\text{argmin}}\ & \text{Cost}_{\text{HD}}(\alpha) \\ \text{s.t}\quad & \text{(PHZD)}, \\ & \text{Physical Constraints}, \end{aligned} \tag{HIO}$$

where the cost function (HIO) is the least-square-fit error between the human experimental data (which are obtained from the IMUs as discussed in Sec. 2.1) and the CWF representations (3). Note that the physical constraints include addition constraints that ensure good foot clearance and that joint limits intrinsic to the prosthetic device are satisfied. The end result of this optimization problem is the parameter set α that renders an optimal (w.r.t. torque, foot clearance, joint position and velocity) and provably stable human-like walking gait, which can be implemented directly on the pros-

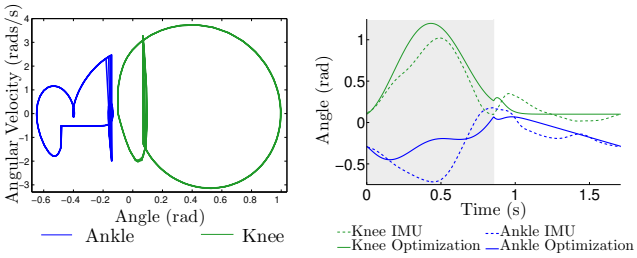

(a) Limit cycles (b) Data Comparison

Figure 3: (a) Limit cycles for both the ankle and knee; (b) Comparison between the collected data and outputs optimized via (HIO); the shadowed region represents the swing phase.

thetic device. The stability of the walking gait obtained through (HIO) was numerically validated through the Poincaré map [25], wherein the magnitude of the maximum eigenvalue was found to be 0.11 indicating stability. The limit cycles of both the ankle and knee are shown in Fig. 3a.

2.3 Prosthetic Trajectory Reconstruction

The result of the optimization problem (HIO) is the parameter set α that define the human-inspired outputs. Via these outputs, we can obtain desired joint angles and angular velocities on the prosthetic device in every iteration through the inverse projection from the PHZD surface. This is achieved through a methodology termed the *PHZD reconstruction* (a detailed derivation can be found in [34]).

In particular, on the PHZD surface, the zero dynamic coordinates can be defined as:

$$\xi_1 = \delta p_{hip}(\theta) := c\theta \tag{6}$$

$$\xi_2 = y_1^a(\theta,\dot{\theta}) := \delta \dot{p}_{hip}(\theta) := c\dot{\theta}, \tag{7}$$

where c is the coefficient array defining the linearized hip position $\delta p_{hip}(\theta)$ [34]. Since the linearized hip position is utilized to parameterize time (4), as the direct result of (6) the desired relative degree two outputs can be stated as $y_2^d(\rho(\theta),\alpha) = y_2^d(\xi_1,\alpha)$. Similarly, due to the linearity of the actual relative degree two outputs, we have $y_2^a = H\theta$ and $\dot{y}_2^a = H\dot{\theta}$.

Therefore, utilizing the fact that the actual outputs are equal to the desired outputs on the PHZD surface, we have the following relationships between the desired joints states and the desired outputs of the robot given by:

$$\theta_d(\xi) = \Psi(\xi_1,\alpha) = \begin{bmatrix} c \\ H \end{bmatrix}^{-1} \begin{pmatrix} \xi_1 \\ y_2^d(\xi_1,\alpha) \end{pmatrix} \tag{8}$$

$$\dot{\theta}_d(\xi) = \Phi(\xi_1,\xi_2,\alpha) = \begin{bmatrix} c \\ H \end{bmatrix}^{-1} \begin{pmatrix} v_{hip} \\ \frac{\partial y_2^d(\xi_1,\alpha)}{\partial \xi_1}\xi_2 \end{pmatrix}.$$

The immediate result of this expression is that with knowing ξ_1 and ξ_2, which are simply the linearized hip position and hip velocity, respectively, the desired angles and velocities can be obtained using the parameter α directly while simultaneously guaranteeing the resulted joint states and velocities are on the PHZD surface. Fig. 3b shows the reconstructed knee and ankle angles compared with the experimental locomotion data obtained from the IMUs. Note that the large negative ankle angle recorded by the IMUs is because flat-footed walking was enforced during the data collection experiment. As a result of this unnatural constraint, the test subject had to increase plantar flexion in order to land with a flat foot. Aside from this difference, the walking gait obtained through the optimization problem (HIO) is human-like in nature.

3. CONTROLLER CONSTRUCTION

In this section, we begin by briefly summarizing impedance control. This traditional control approach will be utilized in the development of a novel *control Lyapunov function* (CLF) [6] based *model independent quadratic program* (MIQP) controller for two joints. This was first proposed in [32], but will be revised with a direct view towards application to prosthesis.

3.1 Impedance Control for Prosthesis

Based on the notion of impedance control in [17], the torque at each joint during a single step can be represented in a piecewise fashion by a series of passive impedance functions [28] of the form:

$$\tau^{imp} = k(\theta - q^e) + b\dot{\theta}, \tag{9}$$

where, k, q^e and b represent the impedance parameters for stiffness, equilibrium angle and damping, respectively, which are constant for a specific phase. This simple formula has two advantages: first, no reference tracking trajectory is required and second, only local information about the controlled prosthetic joints is necessary. Therefore, the end result is a simple prosthesis control that has been vastly favored in powered prosthesis research [12, 21, 28, 29].

Phase Separation and Impedance Estimation. Based upon previous work [3], analysis of flat foot locomotion data obtained from human models shows that one gait cycle can be divided into four subphases (two subphases for the stance phase and two subphases for the swing phase) based on the profile of prosthesis joint angles. The explicit criterion of the phase separation is bypassed here but can be found in [3, 32]. With the phase transitions in hand, the impedance parameters for each subphase are estimated using the method discussed in [3], in which the authors showed that the impedance parameters for a lower-limb prosthesis can be learned by the observation of unimpaired human walkers. The results have been validated both in simulation and in experiment with a transfemoral prosthetic device. In this paper, we extend the method to estimate the impedance parameters by observing the experimental walking data that is obtained using only PD control on the device via (8). The estimation algorithm is discussed explicitly in [3, 32].

3.2 CLF Model Independent QP

As a means for stabilizing systems undergoing impacts, i.e., hybrid systems, rapidly exponentially stabilizing control Lyapunov functions (RES-CLFs) were introduced in [6] to yield controllers with stronger convergence guarantees. Quadratic programs can be used to realize RES-CLFs (via inequality constraints). When combined with the impedance control (implemented as a feed-forward term), the result is a novel feedback control methodology: Model Independent Quadratic Programs (MIQP)+Impedance control.

Human-Inspired Control Revisiedt. With the human-inspired outputs defined in (3), the dynamics in (2) can be reformulated as:

$$\begin{bmatrix} \dot{y}_1 \\ \ddot{y}_2 \end{bmatrix} = \underbrace{\begin{bmatrix} L_f y_1(\theta,\dot{\theta}) \\ L_f^2 y_2(\theta,\dot{\theta}) \end{bmatrix}}_{L_f} + \underbrace{\begin{bmatrix} L_g y_1(\theta,\dot{\theta}) \\ L_g L_f y_2(\theta,\dot{\theta}) \end{bmatrix}}_{A} u, \tag{10}$$

where L_f is the *Lie* derivative and A is the dynamic decoupling matrix, which is invertible because of the specific criterion of the outputs selection [35]. By picking $u = A^{-1}(L_f + \mu)$, equation (10) becomes:

$$\begin{bmatrix} \dot{y}_1 \\ \ddot{y}_2 \end{bmatrix} = \mu. \tag{11}$$

By designing μ properly (see [4]) one can drive both $y_1 \to 0$ and $y_2 \to 0$ exponentially. However, due to the lack of the model in-

formation, it is not possible to realize this controller on prosthesis. As a result, traditional PID control is the more favorable option—it does not require accurate model information, i.e., it is model independent. However, PID controllers lack formal guarantees (when applied to nonlinear systems) and require hand tuning [8]. This motivates the need to find a new control strategy that overcomes the weaknesses of PID control while maintaining model insensitivity. This balance of performance and lack of model-based assumptions was achieved with CLF based MIQP as first introduced in [32].

CLF MIQP. The prosthetic device AMPRO has two actuators for the ankle and knee joints, therefore, is natural to choose the outputs to be the ankle and knee angles. By defining the vector $\eta = (y_p; \dot{y}_p) \in \mathbb{R}^{4\times 1}$ with $y_p = (\theta_a^p, \theta_k^p)^T$, equation (11) can be written as a linear affine control system:

$$\dot{\eta} = \underbrace{\begin{bmatrix} 0_{2\times 2} & I_{2\times 2} \\ 0_{2\times 2} & 0_{2\times 2} \end{bmatrix}}_{F} \eta + \underbrace{\begin{bmatrix} 0_{2\times 2} \\ I_{2\times 2} \end{bmatrix}}_{G} \mu. \tag{12}$$

Note that, θ_a^p and θ_k^p are the angles for the prosthetic ankle joint and knee joint, respectively. By considering the Continuous Algebraic Riccati Equations (CARE) with $P = P^T > 0$:

$$F^T P + PF - PGG^T P + I = 0, \tag{13}$$

we can obtain the optimal solution $\mu = -G^T P \eta$. The solutions of the CARE also allows for the construction of a *rapidly exponentially stabilizing control Lyapunov functions (RES-CLFs)* [7]. In particular, by defining $\eta_\varepsilon = (y_p/\varepsilon; \dot{y}_p)$ with $\varepsilon > 0$, we define the positive definite RES-CLFs to be:

$$V_\varepsilon(\eta) = \eta^T \begin{bmatrix} \frac{1}{\varepsilon} I & 0 \\ 0 & I \end{bmatrix} P \begin{bmatrix} \frac{1}{\varepsilon} I & 0 \\ 0 & I \end{bmatrix} \eta := \eta^T P_\varepsilon \eta. \tag{14}$$

Differentiating this function yields:

$$\dot{V}_\varepsilon(\eta) = L_F V_\varepsilon(\eta) + L_G V_\varepsilon(\eta)\mu, \tag{15}$$

where $L_F V_\varepsilon(\eta) = \eta^T (F^T P_\varepsilon + P_\varepsilon F)\eta$, $L_G V_\varepsilon(\eta) = 2\eta^T P_\varepsilon G$.

In order to exponentially stabilize the system, we want to find μ such that, for specifically chosen $\gamma > 0$ [6], we have:

$$L_F V_\varepsilon(\eta) + L_G V_\varepsilon(\eta)\mu \leq -\frac{\gamma}{\varepsilon} V_\varepsilon(\eta). \tag{16}$$

Therefore, an optimal μ could be found by solving the following quadratic programs (QP):

$$\begin{aligned} m(\eta) = \underset{\mu\in\mathbb{R}^2}{\operatorname{argmin}}\ & \mu^T \mu && (17)\\ \text{s.t}\quad & \varphi_0(\eta) + \varphi_1(\eta)\mu \leq 0, && \text{(CLF)} \end{aligned}$$

where $\varphi_0(\eta) = L_F V_\varepsilon(\eta) + \frac{\gamma}{\varepsilon} V_\varepsilon(\eta)$ and $\varphi_1(\eta) = L_G V_\varepsilon(\eta)$. The end result of solving the QP problem is a control input μ which is independent of model information, i.e., we obtain a MIQP.

More explicitly, the basic principle of the MIQP algorithm is to construct a new linear control system (12) that only focuses on the errors between the actual outputs and desired outputs, while not requiring any information about the original model. Note that, in order to obtain optimal torques that are also subject to other constraints (for example, torque bounds due to hardware limit), we take a further step by relaxing the CLF constraints with a large penalty value $p > 0$ [5]. In particular, we consider the MIQP:

$$\begin{aligned} \underset{(\delta,\mu)\in\mathbb{R}^{2+1}}{\operatorname{argmin}}\ & p\delta^2 + \mu^T \mu && (18)\\ \text{s.t}\quad & \varphi_0(\eta) + \varphi_1(\eta)\mu \leq \delta, && \text{(CLF)}\\ & \mu \leq \mu_{MAX}, && \text{(Max Torque)}\\ & -\mu \leq \mu_{MAX}. && \text{(Min Torque)} \end{aligned}$$

This QP problem yields an optimal controller regulates the error in the output dynamics in a rapidly exponentially stable fashion.

3.3 MIQP+Impedance Control

While MIQP control benefits from its model independent property in an optimal fashion, it also suffers the problems due to the lack of model information. For example, the MIQP controller will generate the same torque of two different systems if they have the same tracking error, regardless of the torque actually required of the system. Therefore, model information must be utilized in the controller in order to achieve a more responsive controller; this motivates the introduction of MIQP+Impedance control.

By viewing the impedance controller τ^{imp} as a feed-forward term, the desired torque τ_d of the prosthetic joints can be stated as:

$$\tau_d = \tau^{qp} + \tau^{imp}, \tag{19}$$

where τ^{qp} is the torque computed from the MIQP problem. Taking this idea further, we add the impedance term τ^{imp} into the MIQP construction for the total hardware torque bounds, which yields the following MIQP+Impedance formula:

$$\begin{aligned} \underset{(\delta,\tau^{qp})\in\mathbb{R}^{2+1}}{\operatorname{argmin}}\ & p\delta^2 + \tau^{qpT}\tau^{qp} && (20)\\ \text{s.t}\quad & \varphi_0(\eta) + \varphi_1(\eta)\tau^{qp} \leq \delta, && \text{(CLF)}\\ & \tau^{qp} \leq \tau^{qp}_{MAX}, && \text{(Max QP Torque)}\\ & -\tau^{qp} \leq \tau^{qp}_{MAX}, && \text{(Min QP Torque)}\\ & \tau^{qp} \leq \tau_{MAX} - \tau^{imp}, && \text{(Max Input Torque)}\\ & -\tau^{qp} \leq \tau_{MAX} + \tau^{imp}. && \text{(Min Input Torque)} \end{aligned}$$

By adding the impedance control as a feed-forward term into the input torque, the model independent dynamic system (12) gathers some information about the system that it is controlling. It can, therefore, adjust τ^{qp} accordingly to accommodate for the feed-forward term in order to achieve good tracking. By setting the QP torque bounds τ^{qp}_{MAX}, we can limit problems with overshoot. We also set the total input torque bounds for the QP problem such that the final optimal input torque (19) will satisfy the hardware torque bounds τ_{MAX}, which is critical for practical implementation.

The astute reader make notice that the final formulation of the MIQP+Impedance controller in this paper is slightly different than previously presented [32, 33]. In particular, instead of adding the feed-forward impedance torque into the QP problem, this work only considers the impedance term in the torque boundary constraints. This important modification is specifically considered because of safety concerns related to prosthesis that interact with humans. In [32, 33], when considering the feed-forward term in the QP problem, the MIQP+Impedance control is solved optimally for the total input torque; for this reason, the resulting optimal torque tends to be as small as possible. However, for prosthesis control where safety is of primary concern, small torques may result in instability or even failure, i.e., the user falling. Therefore, by removing the feed-forward term from the QP problem, we are only optimizing the QP torque while enforcing the total torque bounds

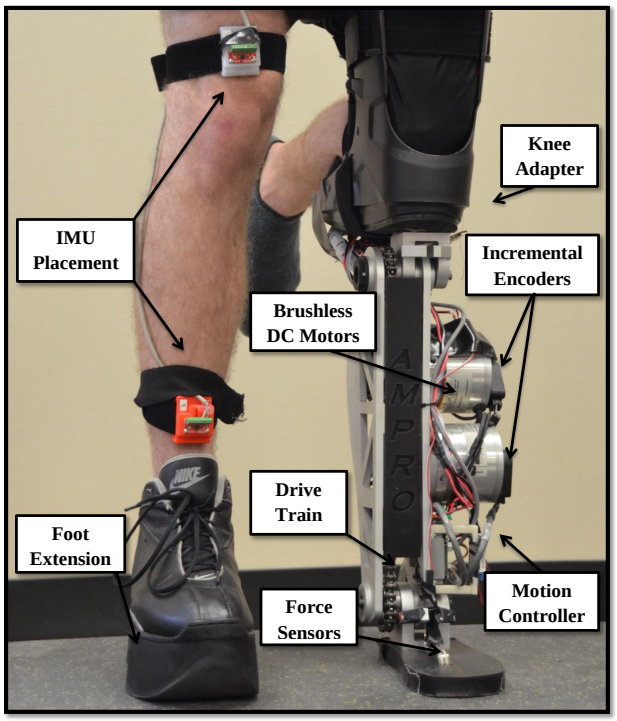

Figure 4: Diagram indicating the different components of AMPRO.

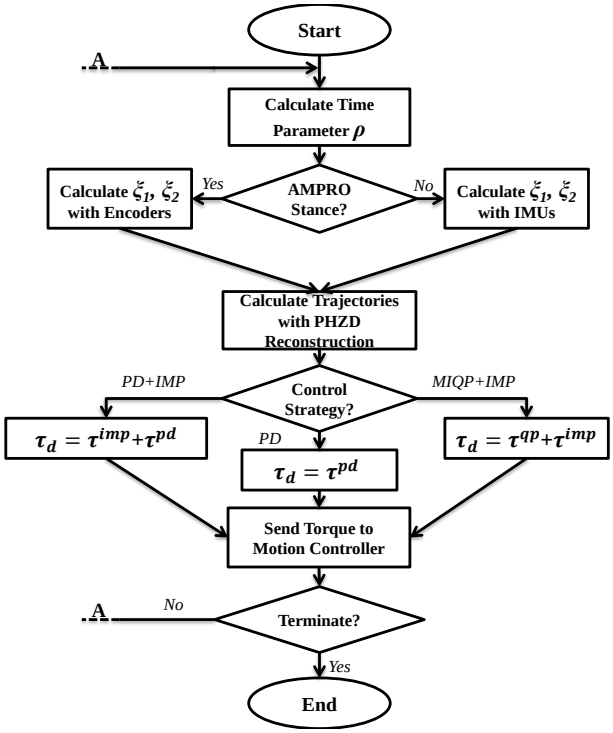

Figure 5: Flow chart of the pseudo-code.

that must be satisfied. The end result is a controller with optimal torque that does not sacrifice safety.

4. EXPERIMENTAL IMPLEMENTATION

With the gait and controller discussed above, we now have the framework to implement the nonlinear real-time optimization based controller experimentally on the self-contained transfemoral prosthesis, AMPRO. Specifically, the design specifications of AMPRO are briefly introduced at the beginning of this section. Then the high level control algorithm along with IMU sensing are explained. Finally, the results of using the MIQP+Impedance controller along with other controllers are analyzed in a comparative study.

4.1 Design Specifications of AMPRO

AMPRO (**AM**BER **Pro**sthetic) was designed to be a high powered, compact and structurally safe device. The device uses a roller chain drive train consisting of a 374 W brushless DC motor (Moog BN34 silencer series) and a harmonic gearhead (Harmonic Drive model CSG-2UH-LW) to actuate the ankle and knee joints in the sagittal plane. This design utilizes two incremental encoders for each motor and is designed to incorporate absolute encoders at both actuated joints. Two Elmo motion controllers are used to drive the motors and read the encoder values. Additionally, two FlexiForce (Parallax 30056) force sensors are located at the base of the foot (mounted at the toe and heel) to measure the normal reaction forces which are used for the purpose of leg switch. The prosthetic device is powered by a 8-cell LiPo battery with 4000 mAh capacity. The technical diagram can be seen in Fig. 4 and the detailed design specifications of AMPRO can be found in [19].

4.2 High Level Control and IMU Sensing

The high-level controller of AMPRO is coded into *C++* packages and run on the Robot Operating System (ROS). The complete code is realized independently with a low-power single-board computers: Beaglebone Black (BBB) at 200 Hz. The pseudo-code of the algorithm is shown as the flowchart in Fig. 5.

IMU Sensing. To provide a point of human-robotic interaction, two IMUs are mounted on the shin and thigh of the human leg. The assumption is made that the user walks flat-footed in the saggital plane, eliminating the use of an IMU on the human foot. The EKF internal model for each IMU is used to obtain relative orientation and velocity between body segments. Information which is directly used for control is knee angle/velocity (thigh to shank) and ankle angle/velocity (shank to earth). While the human leg is in stance, IMU readings are utilized to compute ξ_1 and ξ_2; therefore, the desired swing trajectories of the prosthetic can be calculated accordingly using the method discussed in Sec. 2.3. For hardware implementation, one BBB is dedicated to run the EKF algorithms as introduced in Sec. 2.1. The communication to a second BBB which runs the primary code structure is achieved over a networked crossover cable.

4.3 Experimental Results

Before the implementation of MIQP+Impedance control on the prosthesis, the PD controller (obtained from (8)):

$$\tau^{pd} = -K_p(\theta_a - \theta_d(\xi)) - K_d(\dot{\theta}_a - \dot{\theta}_d(\xi)), \qquad (21)$$

is first realized to track the reconstructed trajectories obtained in Sec. 2 to achieve stable walking. Walking trails were performed on a treadmill providing a constant speed of 1.4 mph which allows increased safety for the human subject (with the use of handrails) and the researchers monitoring experiments. During each experiment, data recorded from the joint sensors and the feedback from the human subject were used to fine tune the controller gains. Finally, a set of controller gains is chosen to realize smooth stable walking while at the same time guaranteeing the best comfortability of

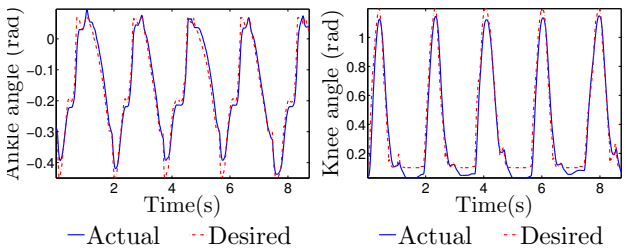

(a) Tracking with PD

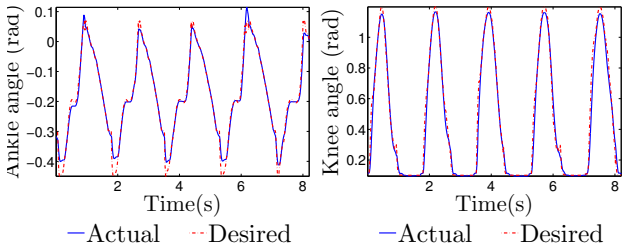

(b) Tracking with MIQP+Impedance with high torque bounds

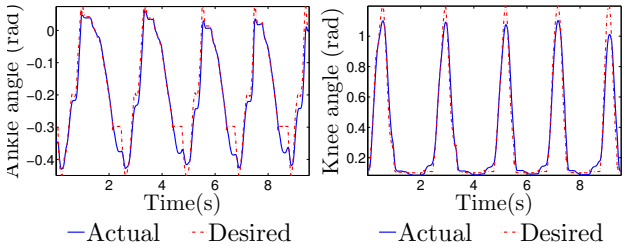

(c) Tracking with MIQP+Impedance with low torque bounds

Figure 6: Tracking results of using PD control and MIQP+Impedance control with HS.

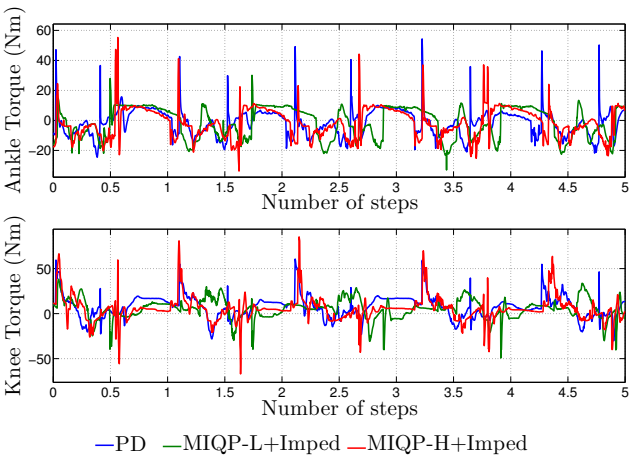

Figure 7: Torque comparisons between using PD control and MIQP+Impedance control with HS.

the human subject. The experimental results will be discussed later when compared with using MIQP+Impedance control. With the estimation algorithm introduced in [32], impedance parameters are then learned based on the experimental walking data obtained using PD control.

MIQP+Impedance Control. With impedance parameters obtained

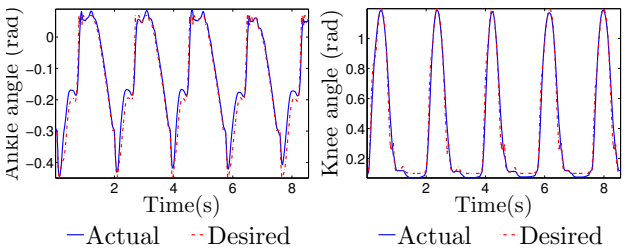

(a) Tracking with PD+Impedance

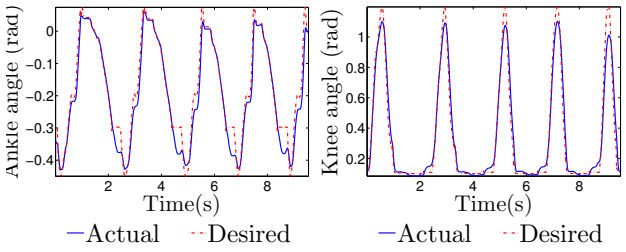

(b) Tracking with MIQP+Impedance with low bounds

Figure 8: Tracking results of using PD control and MIQP+Impedance control with HS.

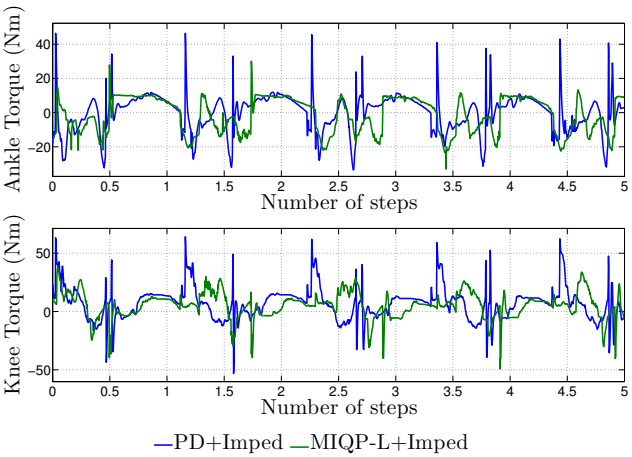

Figure 9: Torque comparisons between using PD control and MIQP+Impedance control with HS.

in the previous section, we apply impedance control as the feed-forward term while using the MIQP (20) as the feedback to track the desired joint trajectories. In particular, for the first round of testing, we set both the torque bounds τ_{MAX}^{qp} and τ_{MAX} to be 100 Nm which is relatively high due to the safety concerns. With this controller, the tracking results of both the ankle and knee are plotted in Fig. 6b along with the results obtained through PD control as shown in Fig. 6a. It is evident that the tracking performance of both the ankle and the knee are exceptionally good for MIQP+Impedance control. Fig. 7 shows the corresponding torques of using these two controllers; the MIQP+Impedance control uses more torque as due to its increased ability to track the desired trajectories.

With the goal of showing the torque optimality of the proposed novel controller, the torque bounds τ_{MAX}^{qp} and τ_{MAX} are reduced to be 50 Nm for the second round of testing. The tracking results of using MIQP+Impedance control with low torque bounds are shown in Fig. 6c. While the tracking performance is not as good as

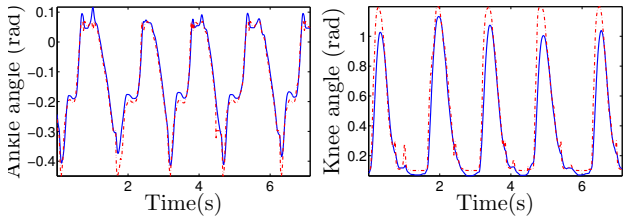

(a) Tracking with PD

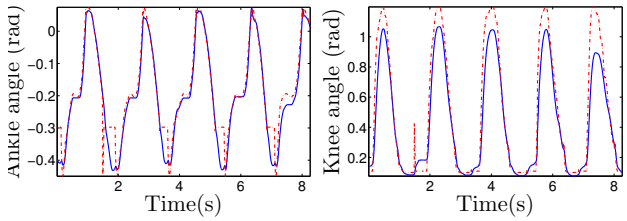

(b) Tracking with MIQP+Impedance with low bounds

Figure 10: Tracking results of using PD+Impedance control and MIQP+Impedance control with NHS.

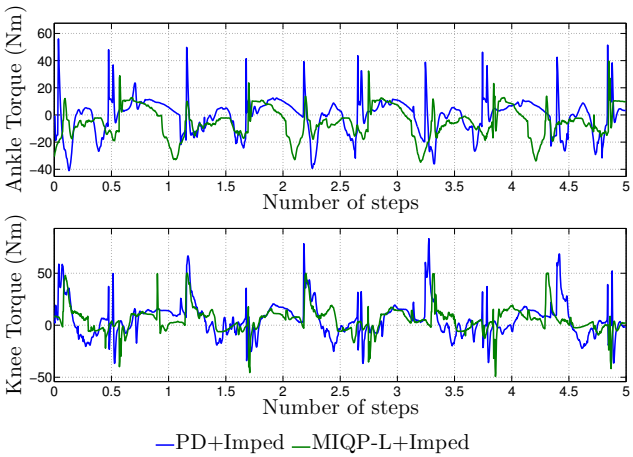

Figure 11: Torque comparisons between using PD+Impedance control and MIQP+Impedance control with NHS.

the tracking with high torque bounds, it is still better than the result with PD control. More importantly, this better tracking is achieved with lower torque when compared to PD control, which is shown in Fig. 7.

Note that, since the test subject is a healthy human, a special knee adapter is utilized for the connection between the test subject and the device, which results in a significant leg asymmetry. For this reason, it is hard to maintain lateral balance especially when there is no support for the test subject. Therefore, for control verification purposes, two test situations are considered. One test case is that the subject is allowed to use hand support (HS), i.e., push or pull a side handrail if the subject is about to lose lateral balance. Importantly, the HS only helps with lateral balance but does not support the test subject in the sagittal plane. Another test case is that the subject walks with no hand support (NHS) at all. When using HS, the subject was found to walk more periodically since there is no issue with lateral stability. The above test results are all with HS. On the other hand, when with NHS, the subject has to balance himself by placing his foot differently in each step. Therefore, the tracking performance is sacrificed and the walking is less periodic, which will be shown in the following section.

Comparison with PD+Impedance Control. While the novel control, MIQP+Impedance, contains both the feedback term and feed-forward term, we also compare it with a more straightforward augmented control strategy, PD+Impedance:

$$\tau^d = \tau^{pd} + \tau^{imp}, \tag{22}$$

which also includes the impedance control as a feed-forward term. The tracking results are compared against using MIQP+Impedance control with low torque bounds for both the HS and NHS cases, which are shown in Fig. 8 and Fig. 10, respectively. For the HS case, we can see that the PD+Impedance control has better tracking than MIQP+Impedance control. As a result, the torques are also bigger for PD+Impedance control, which can be seen in Fig. 9. For the case with NHS, we can see that the tracking performances are similar for the two controllers as shown in Fig. 10. However, the MIQP+Impedance control with low torque bounds achieves this tracking performance with lower torque as shown in Fig. 11.

To illustrate the overall control performance more clearly, the experimental results (including tracking errors, maximum torque requirement and average net power consumption) of 5 steps for the HS case are listed in Table. 1 thereby giving a detailed comparison. In particular, the best performances are highlighted in the table, from which we can see that except the max knee error, all of the best performances are achieved with the MIQP+Impedance controllers. More importantly, compared with PD or PD+Impedance, the proposed novel controller has reduced the torque and power significantly, which is an essential consideration in prosthesis control. In summary, after comparing the different controllers under different situations, the MIQP+Impedance controller has the best balanced performance between tracking and power requirements.

Outdoor Tests. As an additional form of testing, AMPRO was taken out of the lab to walk in various environments. In particular, two tests were performed at the student Recreation Center of Texas A&M University as illustrated in Fig. 12. The first test was carried out using the MIQP+Impedance control with low torque bounds; the test subject was able to walk 30 mins continuously with a total travel distance of $3/4$ miles. The gait tiles are plotted in comparison with the simulated walking as shown in Fig. 13. Testing was prematurely terminated due to an electrical failure on the shin IMU sensor. The battery voltage drop was monitored to estimate the power cost. The voltage drop during the course using the MIQP+Impedance controller for the continuous walking test was 1 V. For comparison purposes, another test was performed employing PD control. The subject successfully finished 1 mile in 40 mins (the average walking speed was similar to the MIQP+Impedance

Table 1: Experiment Results Comparison with Hand Support.

Control		$e_{rms}[rad]$	$e_{max}[rad]$	$\tau_{max}[Nm]$	$P_{rms}[W]$
PD	**Ankle**	0.0311	0.1139	56.4042	9.966
	Knee	0.0817	0.3038	62.2391	34.1918
PD+	**Ankle**	0.033	0.1165	47.5438	15.6797
Imped	**Knee**	0.056	**0.2106**	64.8324	40.9382
MIQP-L	**Ankle**	0.0368	0.1231	**33.0213**	**7.8233**
+Imped	**Knee**	0.0631	0.2292	**49.3158**	**27.5365**
MIQP-H	**Ankle**	**0.0192**	**0.08**	58.4356	9.4622
+Imped	**Knee**	**0.0528**	0.25	85.3194	39.3123

Figure 12: Walking unsupported in the Student Recreation Center.

control walking speed) with 1.5 V voltage drop over the course of the continuous walking experiment. From the voltage drop comparison, we can conclude that the MIQP+Impedance controller required less power during the test of walking freely. A video of the experiments can be seen at [1].

5. CONCLUSIONS

By leveraging a systematic methodology—including sensing, algorithm and control—which has been validated on various bipedal robots, this work has successfully translated robotic walking to prosthetic walking. In particular, a nonlinear real-time optimization based controller (i.e., MIQP+Impedance) was implemented on a custom built powered transeformal prosthesis. Continuous and stable flat ground walking was shown with this novel controller during both in-lab and real-world testing. When compared to other controllers, the proposed MIQP+Impedance controller outperforms PD control in both tracking and torque optimality and displays a well balanced performance (tracking and power requirements) when compared with PD+Impedance control. The rate of power consumption is also improved by the MIQP+Impedance controller when compared to both PD and PD+Impedance. More importantly, by benefiting from both the simple algorithm infrastructure and the optimal control strategy (MIQP), the self-contained prosthesis was estimated to have a continuous walking capacity of more than 3 hours on a single battery charge. A new design of AMPRO is currently focused on reducing the size of the electric motors and optimizing other structural components with the aim of providing a more comfortable experience for the user and to significantly reduce power consumption. Future work will be focused on the realization of a multi-contact walking gaits (as realized on bipedal robots in [34]) to achieve more natural human-like walking with respect to torque and ground reaction forces.

Acknowledgement

This research is supported under: NSF CAREER Award CNS-0953823 and Texas Emerging Technology Fund 11062013. This research has approval from the Institutional Review Board with IRB2014-0382F for testing with human subjects.

6. REFERENCES

[1] AMPRO walks with the nonlinear real-time optimization controller. `http://youtu.be/NxJ7nMsJ63o`.

[2] Comparison of mechanical energy expenditure of joint moments and muscle forces during human locomotion. *Journal of Biomechanics*, 29(4):405 – 415, 1996.

[3] N. Aghasadeghi, H. Zhao, L. J. Hargrove, A. D. Ames, E. J. Perreault, and T. Bretl. Learning impedance controller parameters for lower-limb prostheses. *IEEE: IROS*, 2013.

[4] A. D. Ames. First steps toward automatically generating bipedal robotic walking from human data. In *Book chapter of Robotic Motion and Control*, volume 422, pages 89–116, 2011.

[5] A. D. Ames. Human-inspired control of bipedal robots via control lyapunov functions and quadratic programs. In *16th International conference on Hybrid systems: computation and control*, pages 31–32. ACM, 2013.

[6] A. D. Ames, K. Galloway, and J. Grizzle. Control lyapunov functions and hybrid zero dynamics. In *Decision and Control (CDC), 2012 IEEE 51st Annual Conference on*, pages 6837–42.

[7] A. D. Ames, K. Galloway, J. Grizzle, and K. Sreenath. Rapidly exponentially stabilizing control lyapunov functions and hybrid zero dynamics. 2014.

[8] D. Atherton and S. Majhi. Limitations of pid controllers. In *American Control Conference*, pages 3843–3847, 1999.

[9] C. G. Atkeson and S. Schaal. Robot learning from demonstration. In *ICML*, pages 12–20, 1997.

[10] S. Au, M. Berniker, and H. Herr. Powered ankle-foot prosthesis to assist level-ground and stair-descent gaits. *Neural Networks*, 21(4):654 – 666, 2008.

[11] S. Au, P. Bonato, and H. Herr. An emg-position controlled system for an active ankle-foot prosthesis: an initial experimental study. In *Rehabilitation Robotics, 2005. 9th International Conference on*, pages 375–379.

[12] J. A. Blaya and H. Herr. Adaptive control of a variable-impedance ankle-foot orthosis to assist drop-foot gait. *Neural Systems and Rehabilitation Engineering, IEEE Transactions on*, 12(1):24–31, 2004.

[13] A. Boehler, K. Hollander, T. Sugar, and D. Shin. Design, implementation and test results of a robust control method for a powered ankle foot orthosis (afo). In *Robotics and Automation, ICRA, IEEE*, pages 2025–2030, 2008.

[14] W. Flowers and R. Mann. Electrohydraulic knee-torque controller for a prosthesis simulator. *ASME J. of Biomechanical Engineering*, 99(no.4):pp.3–8, 1977.

[15] F. W. C. Grimes D. L. and D. M. Feasibility of an active control scheme for above knee prostheses. *ASME J. of Biomechanical Engineering*, 99(no.4):pp.215–221, 1977.

[16] J. Hitt, A. M. Oymagil, T. Sugar, K. Hollander, A. Boehler, and J. Fleeger. Dynamically controlled ankle-foot orthosis (dco) with regenerative kinetics: incrementally attaining user portability. In *Robotics and Automation, 2007 IEEE International Conference on*, pages 1541–1546. IEEE, 2007.

[17] N. Hogan. Impedance control: An approach to manipulation. pages 304–313, 1984.

[18] K. Hollander and T. Sugar. A robust control concept for robotic ankle gait assistance. In *Rehabilitation Robotics, ICORR, IEEE 10th International Conference on*, pages 119–123, 2007.

[19] J. Horn, J. Reher, H. Zhao, V. Paredes, and A. Ames. Ampro: Translating robotic locomotion to a powered transfemoral prosthesis. Seattle, 2014. In proceeding of IEEE: International Conference of Robotic and Automation.

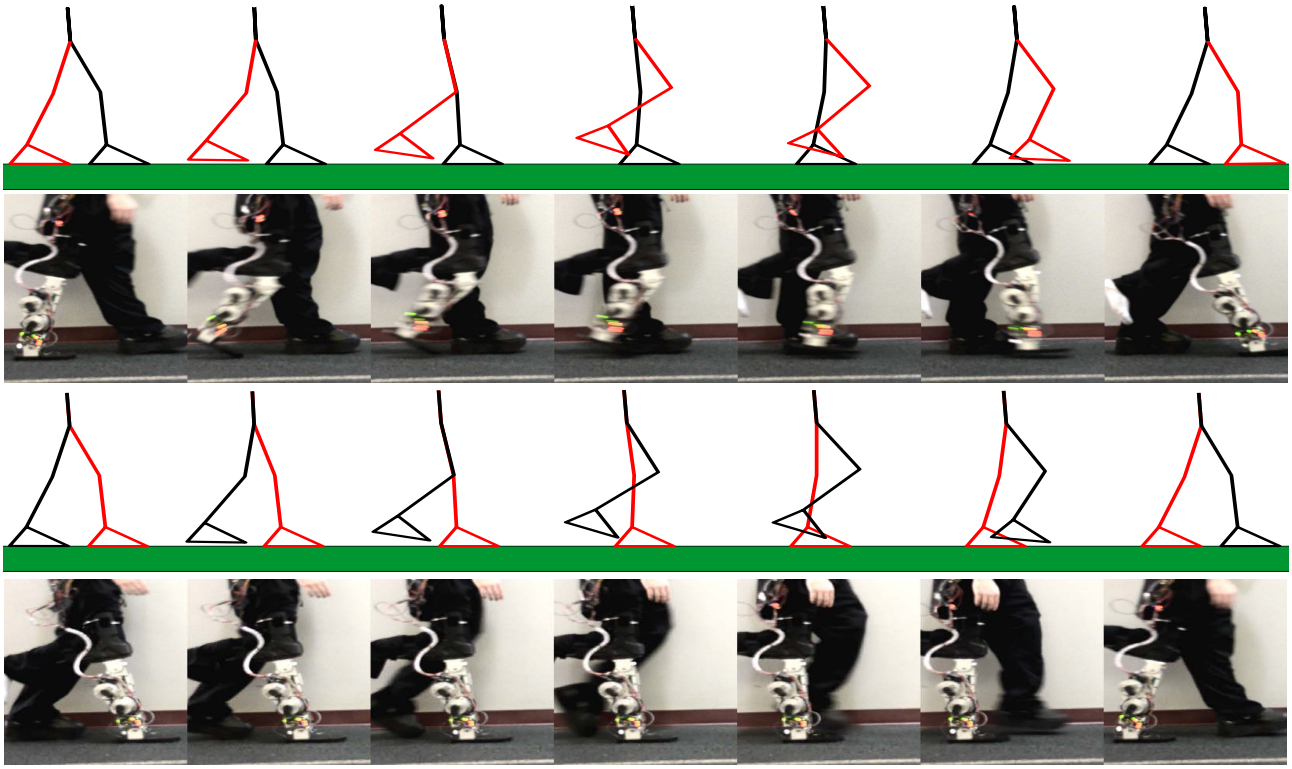

Figure 13: Gait tile comparison between the outside NHS experimental walking and the simulated walking.

[20] Y. Hürmüzlü and D. B. Marghitu. Rigid body collions of planar kinematic chains with multiple contact points. *Intl. J. of Robotics Research*, 13(1):82–92, Feb. 1994.

[21] H. Kawamoto, S. Lee, S. Kanbe, and Y. Sankai. Power assist method for hal-3 using emg-based feedback controller. In *Systems, Man and Cybernetics, 2003. IEEE International Conference on*, volume 2, pages 1648–1653. IEEE, 2003.

[22] W. Ma, H. Zhao, S. Kolathaya, and A. D. Ames. Human-inspired walking via unified pd and impedance control. In *submitted to the IEEE International Conference on Robotics and Automation*, 2014.

[23] J. Nakanishi, J. Morimoto, G. Endo, G. Cheng, S. Schaal, and M. Kawato. Learning from demonstration and adaptation of biped locomotion. *Robotics and Autonomous Systems*, 47(2):79–91, 2004.

[24] A. M. Oymagil, J. K. Hitt, T. Sugar, and J. Fleeger. Control of a regenerative braking powered ankle foot orthosis. In *Rehabilitation Robotics, 2007. ICORR 2007. IEEE 10th International Conference on*, pages 28–34.

[25] T. S. Parker, L. O. Chua, and T. S. Parker. *Practical numerical algorithms for chaotic systems*. Springer New York, 1989.

[26] S. S. Sastry. *Nonlinear Systems: Analysis, Stability and Control*. Springer, New York, June 1999.

[27] S. Šlajpah, R. Kamnik, and M. Munih. Kinematics based sensory fusion for wearable motion assessment in human walking. *Computer methods and programs in biomedicine*, 2013.

[28] F. Sup, A. Bohara, and M. Goldfarb. Design and Control of a Powered Transfemoral Prosthesis. *The International journal of robotics research*, 27(2):263–273, Feb. 2008.

[29] H. A. Varol, F. Sup, and M. Goldfarb. Real-time gait mode intent recognition of a powered knee and ankle prosthesis for standing and walking. In *Biomedical Robotics and Biomechatronics, 2008. BioRob 2008. 2nd IEEE RAS & EMBS International Conference on*, pages 66–72. IEEE, 2008.

[30] D. A. Winter. *Biomechanics and motor control of human gait: normal, elderly and pathological*. 1991.

[31] D. A. Winter and S. E. Sienko. Biomechanics of below-knee amputee gait. *Journal of Biomechanics*, 21(5):361 – 367, 1988.

[32] H. Zhao and A. Ames. Quadratic program based control of fully-actuated transfemoral prosthesis for flat-ground and up-slope locomotion. In *American Control Conference (ACC), 2014*, pages 4101–4107, June 2014.

[33] H. Zhao, S. Kolathaya, and A. D. Ames. Quadratic programming and impedance control for transfemoral prosthesis. In *International Conference on Robotics and Automation (ICRA) 2014*, June.

[34] H. Zhao, W.-L. Ma, M. Zeagler, and A. Ames. Human-inspired multi-contact locomotion with amber2. In *Cyber-Physical Systems (ICCPS), 2014 ACM/IEEE International Conference on*, pages 199–210, April 2014.

[35] H. Zhao, M. J. Powell, and A. D. Ames. Human-inspired motion primitives and transitions for bipedal robotic locomotion in diverse terrain. *Optimal Control Applications and Methods*, 2013.